Correspondence to:
J. J. Boldú,
jordi.boldu@irfu.se

Ion-Acoustic Waves Associated With Interplanetary Shocks

J. J. Boldú[1,2] ![ID], D. B. Graham[1] ![ID], M. Morooka[1] ![ID], M. André[1] ![ID], Yu. V. Khotyaintsev[1] ![ID], A. Dimmock[1], D. Píša[3], J. Souček[3] ![ID], M. Maksimovic[4], P. Louarn[5] ![ID], A. Fedorov[5], G. Nicolaou[6] ![ID], and C. Owen[6] ![ID]

[1]Swedish Institute of Space Physics (IRF), Uppsala, Sweden, [2]Department of Physics and Astronomy, Uppsala University, Uppsala, Sweden, [3]Institute of Atmospheric Physics of the Czech Academy of Sciences, Prague, Czechia, [4]LESIA, Observatoire de Paris, Université PSL, CNRS, Sorbonne Université, University Paris Diderot, Sorbonne Paris Cité, Meudon, France, [5]Institut de Recherche en Astrophysique et Planétologie, CNRS, Université de Toulouse, CNES, Toulouse, France, [6]Mullard Space Science Laboratory, University College London, Surrey, UK

Abstract Ion-acoustic waves (IAWs) commonly occur near interplanetary (IP) shocks. These waves are important because of their potential role in the dissipation required for collisionless shocks to exist. We study IAW occurrence statistically at different heliocentric distances using Solar Orbiter to identify the processes responsible for IAW generation near IP shocks. We show that close to IP shocks the occurrence rate of IAW increases and peaks at the ramp. In the upstream region, the IAW activity is highly variable among different shocks and increases with decreasing distance from the Sun. We show that the observed currents near IP shocks are insufficient to reach the threshold for the current-driven instability. We argue that two-stream proton distributions and suprathermal electrons are likely sources of the waves.

Plain Language Summary Ion-acoustic waves (IAWs) are fluctuations in the electric field that occur at frequencies close to the ion plasma frequency. These waves are commonly found in the solar wind and often cluster around interplanetary (IP) shock waves. In this study, we investigate and quantify how common IAWs are in the vicinity of IP shocks. Our research revealed that IAW activity is enhanced before and after most IP shock passages. Furthermore, IAWs are more likely to be observed preceding IP shocks that are closer to the Sun. We find that the occurrence rate of IAWs shows no clear dependence on the IP shock parameters. We explore the possible mechanisms that could explain the presence of these IAWs. For instance, IAW modes can be excited by electric currents if the associated drift velocity between ions and electrons is above a certain threshold. However, the currents alone are not strong enough to generate the IAWs found near IP shocks. We discuss other potential generation mechanisms, such as velocity distributions of ions and electrons deviating from thermodynamic equilibrium.

1. Introduction

Ion-acoustic waves (IAW) are electrostatic waves commonly observed in the solar wind (Briand, 2009; Gurnett & Anderson, 1977; Gurnett & Frank, 1978). These waves are excited around the proton plasma frequency (f_{pp}) and Doppler-shifted by the solar wind in the spacecraft frame. The main theories regarding their generation involve instabilities driven by electron heat fluxes (Forslund, 1970), strong electric currents (Fried & Gould, 1961), or two-stream protons (Gary, 1978). Solar wind IAWs are of interest as they may play a significant role in the evolution of the ion and electron velocity distribution functions (VDFs). Moreover, the study of IAWs near interplanetary (IP) shocks is important because collisionless shocks require dissipation, which can be provided through wave-particle interactions (Bale et al., 2002; Fitzenreiter et al., 2003). If IAWs provide dissipation, understanding their generation could provide insight into the physics of the shock.

Enhancements in solar wind IAW activity have been demonstrated near IP shocks (Hess et al., 1998; Kurth et al., 1979; Wilson et al., 2007). These enhancements can persist for several hours upstream and downstream of IP shocks (Hess et al., 1998). However, it is not fully understood how far from its ramp an IP shock can influence the excitation of IAWs. Interplanetary shocks observed by the Ulysses and WIND spacecraft, at distances ≥1 AU, do not show any correlation between different shock parameters and IAW activity (Hess et al., 1998; Wilson et al., 2007). Now, with spacecraft exploring the inner heliosphere, it is possible to extend these studies to distances closer to the Sun.

Yu. V. Khotyaintsev, A. Dimmock,
D. Píša, J. Souček, M. Maksimovic,
P. Louarn, A. Fedorov, G. Nicolaou,
C. Owen

Project administration: D. B. Graham,
M. Morooka, M. André,
Yu. V. Khotyaintsev

Resources: J. J. Boldú, D. B. Graham,
Yu. V. Khotyaintsev, A. Dimmock,
D. Píša, J. Souček, M. Maksimovic,
P. Louarn, A. Fedorov, G. Nicolaou,
C. Owen

Software: J. J. Boldú, D. B. Graham,
Yu. V. Khotyaintsev, A. Dimmock,
D. Píša, J. Souček, P. Louarn, A. Fedorov,
C. Owen

Supervision: D. B. Graham, M. Morooka,
M. André, Yu. V. Khotyaintsev

Validation: J. J. Boldú, D. B. Graham,
M. André, Yu. V. Khotyaintsev,
A. Dimmock, D. Píša, J. Souček,
G. Nicolaou

Visualization: D. B. Graham,
M. Morooka, M. André,
Yu. V. Khotyaintsev, A. Dimmock,
G. Nicolaou

Writing – original draft: J. J. Boldú,
D. B. Graham, M. Morooka, M. André,
Yu. V. Khotyaintsev

Writing – review & editing: J. J. Boldú,
D. B. Graham, M. Morooka, M. André,
Yu. V. Khotyaintsev, A. Dimmock,
D. Píša, J. Souček, G. Nicolaou

Assuming Maxwellian proton and electron VDFs with a relative drift, IAWs are strongly damped at low electron-to-ion temperature (T_e/T_i) ratios (Gary, 1978). However, solar wind IAWs are often observed in regions with low T_e/T_i (Briand, 2009). Therefore, it is necessary to investigate the effects of non-Maxwellian VDFs on the ion-acoustic instability T_e/T_i threshold. Non-Maxwellian features like double-proton streams (Alterman et al., 2018; Goldstein et al., 2000) or the electron strahl, a field-aligned electron beam (Verscharen et al., 2019), are common in the solar wind proton and electron VDFs, respectively. Both of these features are potential sources of ion-acoustic instabilities, through the ion-ion instability (Gary, 1993; Treumann & Baumjohann, 1997) and the heat flux instability (Forslund, 1970; Treumann & Baumjohann, 1997), respectively.

In this letter, we investigate IAWs occurring near IP shocks in the inner heliosphere. We find that the IAW occurrence peaks at the shock ramp and can remain enhanced upstream and downstream of the shock. We discuss the source of these waves and to what extent the enhancement in IAWs is due to the presence of the IP shocks.

2. Instrumentation and Data Analysis

We identify IAWs using the Radio and Plasma Waves-Time Domain Sampler (RPW-TDS) instrument (Maksimovic et al., 2020; Soucek et al., 2021), onboard the Solar Orbiter (SolO) spacecraft (Müller et al., 2020). We use two data sets provided by RPW-TDS. First, onboard Triggered Snapshot Waveforms (TSWF) containing high-resolution electric field measurements with typical cadence of 262.1 kHz. Second, statistical data products (STAT) containing 16 s averaged quantities based on snapshots sampled every second. If a snapshot contains a wave, its properties are stored. Every STAT packet is completed after 16 s, and its total number of waves and average quantities are computed, including median frequency and maximum amplitude (Soucek et al., 2021).

In the solar wind, $f_{pp} \sim 0.3$–1 kHz (Píša et al., 2021; Verscharen et al., 2019). Furthermore, Píša et al. (2021) recently showed that the Doppler effect caused by solar wind convection can shift the frequency of IAWs in the spacecraft frame up to 20 kHz. Below this frequency and above f_{pp} the only lightly damped electrostatic waves with wavevector aligned with the magnetic field are IAWs and Langmuir waves when the density is lower than ~ 5 cm^{-3} (Gary, 1993). To determine if a TSWF contains an IAW we perform a fast Fourier transform. If the peak wave power is two orders of magnitude above the background power and at a frequency below 20 kHz, then we identify the TSWF as containing an IAW (Graham et al., 2021). Similarly, if the median frequency from the STAT packet is below 20 kHz, we identify the waves in the STAT packet as IAWs. To avoid including Langmuir waves, we check that the electron plasma frequency at the times of the wave observations is well above 20 kHz.

Magnetic field (**B**) measurements are obtained from the Magnetometer (MAG) instrument with a cadence of 8 vectors/s (Horbury et al., 2020). The Solar Wind Analyzer (SWA) instrument suite (Owen et al., 2020) provides VDF measurements. We use ion VDFs and moments generated by the Proton-Alphas Sensor (PAS) every 4 s and electron pitch angle distribution and moments delivered by the Electron Analyzer System every 10 s.

We focus on IAWs found within ± 200 min of IP shocks. We use this interval to ensure we capture the increase in IAW activity near the IP shocks and determine how far this enhancement extends from the shock. We analyzed 80 IP shocks compiled through an automatic search using data from MAG and PAS (Dimmock et al., 2023). Of these, 15 events were identified through visual inspection when PAS or MAG data were unavailable. The shock parameters are calculated using fixed upstream and downstream intervals according to Kilpua et al. (2015). We present two examples of IP shocks in Figure 1. The shock ramps are highlighted in red. The shock in panels (a)-(e) was observed at 0.71 AU with Alfvén Mach number $M_A = 1.8$ and a shock normal angle $\theta_{BN} = 44°$. This shock has high IAW activity in the upstream region and negligible IAWs downstream, as indicated by the TSWF and STAT measurements in panels (d and e), respectively. The shock in panels (f–j), observed at 0.87 AU, has $M_A = 4.1$ and $\theta_{BN} = 58°$. In this case, IAWs are present on the downstream side and almost no IAWs in the upstream region (panels i and j). In both cases, IAWs are detected at the shock ramps.

3. Results

We begin the analysis by statistically investigating how common IAWs are in the vicinity of IP shocks. We search for any correlation between the occurrence rate of IAWs and IP shock parameters. Then, we analyze possible sources of these waves and their relation to shock physics.
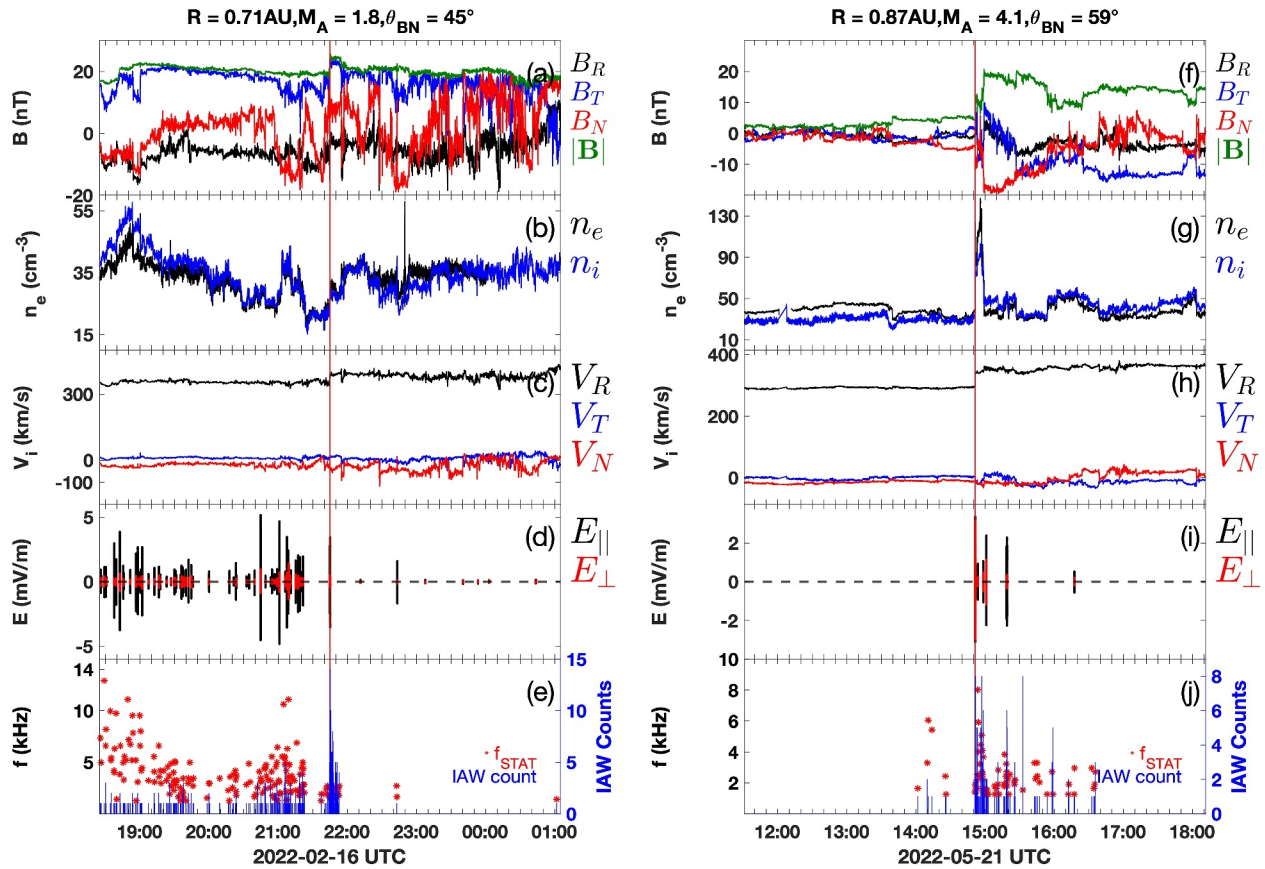
Figure 1. Two examples of IP shocks observed by SolO. (a, f) Magnetic field in RTN (radial, tangential, normal) coordinates. (b, g) Ion density (blue) and electron density from RPW (Khotyaintsev et al., 2021) (black), differences in densities are due to the calibration of the different instruments. (c, h) Ion velocity in RTN coordinates. (d, i) Electric field triggered snapshots in components parallel and perpendicular to the projection of **B** in the antenna plane. (e, j) Median frequency in red asterisk and Ion-acoustic wave counts from STAT data product represented by the blue bars. One STAT packet can have at most 16 waves.

3.1. Statistics of Ion-Acoustic Waves Near Interplanetary Shocks

We define the occurrence rate of IAWs (OR) as

$$OR = \frac{\text{\# of snapshots with IAW in interval}}{\text{total \# of snapshots in interval}}. \tag{1}$$

We use the continuous STAT data to compute OR. To compute OR in the ramp regions, we selected intervals of ± 16 s around the shock crossings. We chose this interval so that there are two STAT packets associated with each ramp.

In Figure 2a, we show the OR of all shocks, where $t = 0$ indicates the time of the shock ramp. The shocks are presented such that negative (positive) times correspond to the upstream (downstream) side, for both fast-forward and fast-reverse shocks (Kilpua et al., 2015). The gray lines on the left axis indicate the OR of each shock, while the blue histogram on the right axis refers to the mean OR for all shocks. We compute the average OR of all IAWs in the solar wind, which is plotted as the red-dashed line on the right axis and has a value of $\sim 0.1\%$. In the ± 16 s ramp interval, 84% of the shocks show enhanced OR compared to the unperturbed solar wind, indicating that IAWs are a common feature of most shock ramps. Moreover, the highest rates occur near the shock ramp, where the mean OR is $\approx 10\%$. Some events reach more than 50%. In the ± 200 min interval from the ramp, 77% of the IP shocks show a higher total OR than the average solar wind.

Upstream, the OR is highly variable among shocks, while downstream the OR is more uniform and decreases rapidly with distance from the ramp. On both sides of the shock, the mean OR increases rapidly around 50 min
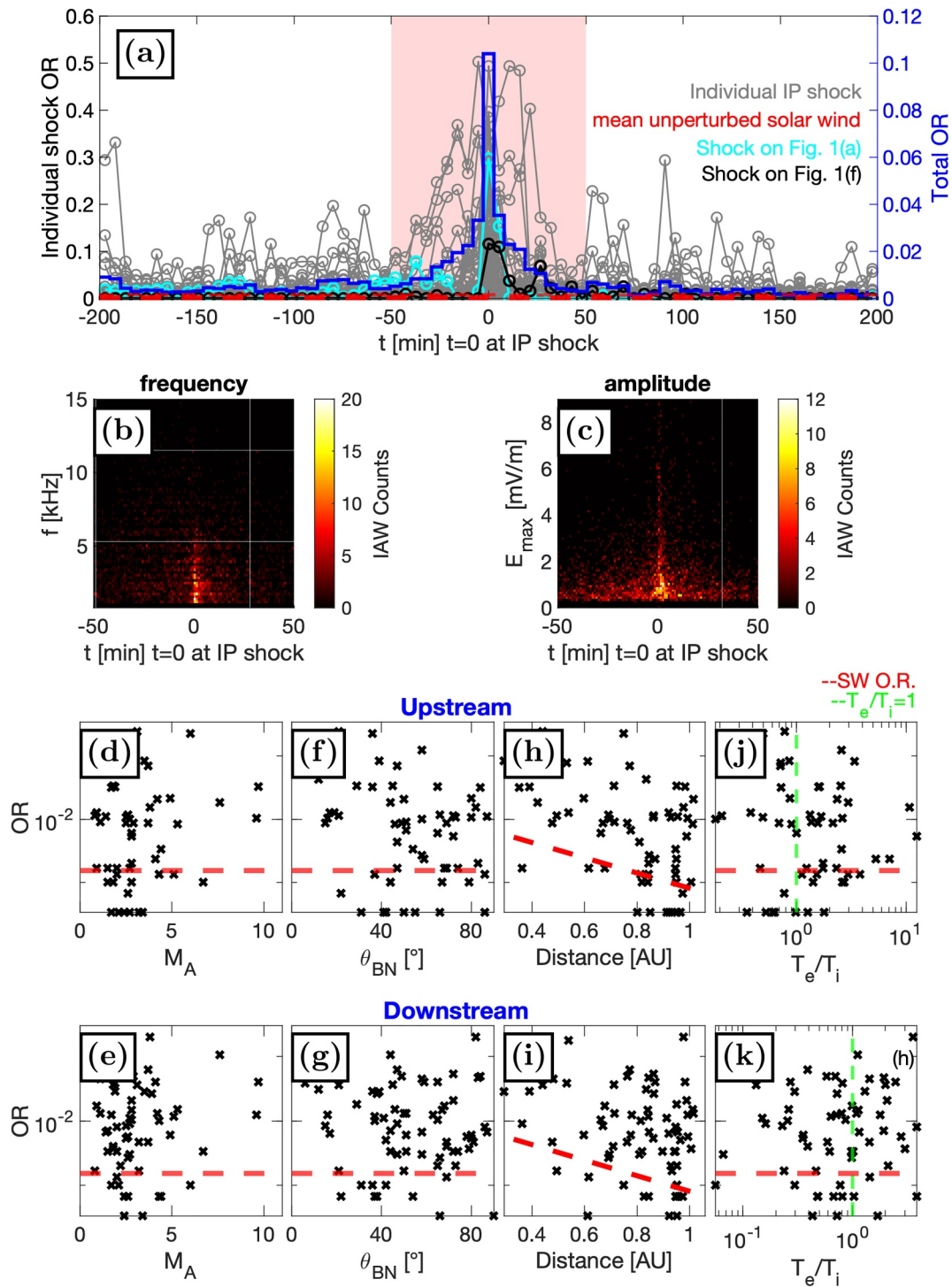
Figure 2. Superposed epoch analysis of the occurrence rate of Ion-acoustic waves (IAWs) (OR) in the vicinity of IP shocks. $t = 0$ corresponds to the time at the shock ramp. Negative (positive) times indicate upstream (downstream) from the ramp. (a) OR across the shocks. The gray lines indicate the OR of each shock and are labeled on the left axis. The blue line and dashed-red line correspond to the mean OR of all shocks and mean solar wind OR, respectively, and are labeled on the right axis. The red-shaded area corresponds to an interval of ±50 min, where the mean OR begins to deviate consistently from the background OR. Panels (b–k) show data from this region. The cyan and black lines show the OR of the IP shock examples in Figures 1a–1j, respectively. (b) Frequency of IAWs. (c) Maximum amplitude of IAWs. (d–k) Scatter plots of shock parameters versus OR. Each cross represents a shock. Panels (d–g) show upstream OR with intervals starting at −50 min and ending 16 s before the ramp passage. Panels (h–k) show downstream OR with intervals starting 16 s after the ramp passage and ending at +50 min. The red-dashed lines indicate the unperturbed solar wind average OR. (d, h) M_A versus OR (e, i) θ_{BN} versus OR (f, j) Distance from the Sun versus OR, the red-dashed lines indicate unperturbed solar wind OR as a function of heliocentric distance (g, k) T_e/T_i versus OR. The vertical green-dashed lines indicate $T_e/T_i = 1$.

from the ramp, as indicated by the red-shaded area in Figure 2a. Closer to the ramp, around ±5 min, the OR in the downstream regions is higher for most shocks than the upstream OR.

Figures 2b and 2c show that IAWs closer to the ramp reach higher frequencies and amplitudes. The frequency of IAWs a few minutes downstream of the ramp, typically remains high, suggesting that the downstream IAWs close to the ramp are related to the shock itself. On the upstream side, the frequency of the waves statistically decreases with distance from the ramp.

For most of the IAWs, the angle between the wave polarization axis and the projected **B**-field is near 0°, indicating propagation predominantly along **B**. This is evident in the examples shown in Figures 1d and 1i where $E_\parallel \gg E_\perp$. Such observations are consistent with earlier findings on IAWs in the solar wind (Gurnett et al., 1979; Lalti et al., 2023; Píša et al., 2021).

Figures 2d–2k shows the relationship between OR and different shock parameters for the upstream and downstream regions. For these plots, we selected, according to Figure 2a, the interval where the mean OR significantly deviates from the unperturbed solar wind OR, indicated by the red-shaded region. The upstream (downstream) regions correspond to the times before (after) the shock passage, excluding the ±16 s of the ramp. In panels (d-g) the upstream OR is plotted for each shock versus M_A, θ_{BN}, heliocentric distance (R), and T_e/T_i. The downstream plots are shown in panels (h–k). For the temperature ratios in panels (g, k), we took an empirical value of T_e = 13.5 eV (Newbury et al., 1998) because electron moments are not yet available for all shocks. This assumption is reasonable as the variations of T_e/T_i are mainly governed by the ion temperature (Briand, 2009).

For the range of IP shock parameters available, no clear dependence of OR on any shock parameter was found, consistent with previous studies at ≥1 AU (Hess et al., 1998; Wilson et al., 2007). We observe a slight correlation between upstream OR and R, with OR tending to increase as R decreases (Figure 2f). This is likely because IAWs are more common closer to the Sun, regardless of the presence of IP shocks (Píša et al., 2021).

In several events, a significant OR enhancement above the background is observed when $T_e/T_i < 1$, where strong IAW damping is expected (Gary, 1978). The enhancement is clearer in the downstream region, where about half of the events have increased OR at $T_e/T_i < 1$ compared to the background OR (Figure 2k). Moreover, $T_e/T_i > 1$ is not sufficient to increase IAW activity, as some shocks with high T_e/T_i do not show any clear enhancement in OR. Other parameters such as upstream plasma β, shock speed, compression ratio, and upstream solar wind speed show no correlation with OR (not shown). Furthermore, no clear dependence of OR on shock parameters was found in the ramp intervals.

3.2. Analysis of Current-Driven Instability

A common instability that leads to IAWs is the current-driven instability, produced by the relative drift between ions and electrons (Christoffersen et al., 1974; Fried & Gould, 1961). At high T_e/T_i, the current-driven instability can lead to wave growth if the drift velocity (v_d) exceeds the ion-sound speed (c_{ia}). At lower T_e/T_i, the instability threshold is increased to larger v_d/c_{ia} (Treumann & Baumjohann, 1997). We estimate v_d through the current density **J** using (Graham et al., 2021):

$$J_T = -\frac{1}{\mu_0} \frac{\Delta B_N}{V_{sw}\Delta t}, \ J_N = \frac{1}{\mu_0} \frac{\Delta B_T}{V_{sw}\Delta t}, \tag{2}$$

where B_T and B_N are the tangential and normal components of the magnetic field in the RTN frame, respectively, Δt is the time step of the MAG measurements, μ_0 is the permeability of free space, and V_{sw} is the solar wind velocity from PAS interpolated to MAG's resolution. Then, v_d is determined from $\mathbf{J} = en\mathbf{v}_d$, where e is the elementary charge. We assume the convection of the current structures by V_{sw} and $J_R = 0$. If the direction normal to the current sheet is not in the radial direction, **J** will be underestimated.

We calculate v_d/c_{ia} and T_e/T_i within ±200 min from the shock ramp and compare with the current-driven instability threshold (Figure 3a). For Maxwelian distributions, the v_d/c_{ia} threshold for wave growth γ can be expressed as (Gurnett & Bhattacharjee, 2017; Treumann & Baumjohann, 1997)
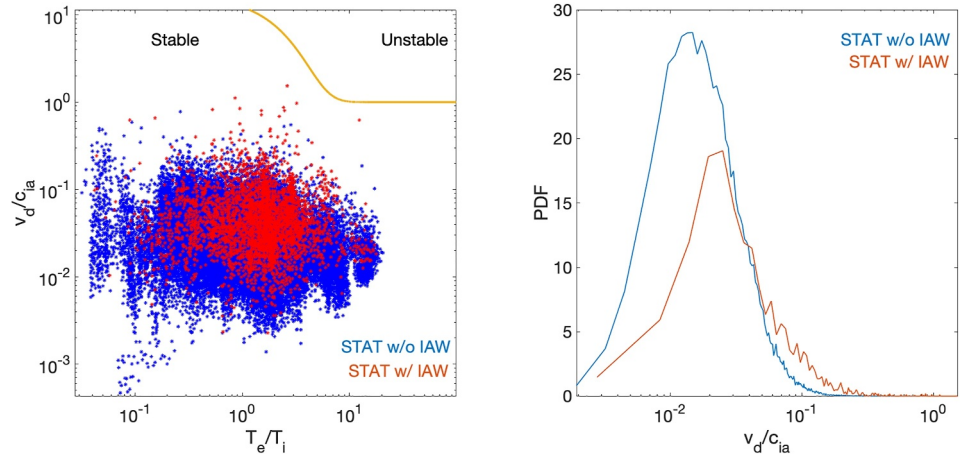
Figure 3. Current-driven instability analysis of the plasma around IP shocks. (a) Scatter plot of v_d/c_{ia} and T_e/T_i of all points (blue) and all Ion-acoustic waves (IAWs) (red) at ±200 min from the IP shocks. The yellow line indicates the boundary between unstable and stable ($\gamma = 0$) values of v_d/c_{ia} for a given T_e/T_i. (b) Probability distribution function of all measurements (blue) and IAW (red) times in terms of v_d/c_{ia}.

$$\frac{v_d}{c_{ia}} = \frac{(3 + T_e/T_i)^{5/2}}{9 + T_e/T_i} \exp\left(\left[-\frac{T_e}{T_i} - \frac{3}{2}\right] \frac{1}{1 + k^2\lambda_D^2}\right)\sqrt{\frac{m_p}{m_e}} + 1, \tag{3}$$

where m_p/m_e is the proton-to-electron mass ratio, k is the wave number, and λ_D is the Debye length. This threshold is indicated with the yellow curve for the long-wavelength limit ($k\lambda_D \ll 1$) in Figure 3a. The blue (red) dots in Figure 3a indicate the values of v_d/c_{ia} and T_e/T_i at the times of STAT packets without (with) IAWs. Since we used STAT data, we took the highest value of v_d/c_{ia} and the mean T_e/T_i in the 16 s STAT packet time interval.

Except for a few exceptional points, the currents are not large enough to reach the instability threshold, even for the largest values of T_e/T_i. We show the histogram of v_d/c_{ia} in Figure 3b. The histogram of STAT packets with IAW is slightly shifted toward higher v_d/c_{ia} compared to the one with no IAWs. Although the estimated currents alone may not lead to IAW instability near IP shocks, on average IAWs are observed in regions of higher v_d.

We note that MAG may under-resolve the thinnest, and likely strongest, proton-scale current sheets. However, previous studies on current sheets in the solar wind showed that v_d is statistically lower than the local Alfvén speed v_A (Lotekar et al., 2022; Vasko et al., 2022). Replacing v_d with the local v_A, the ratio v_A/c_{ia} is on average around an order of magnitude larger than our values of v_d/c_{ia}, but v_A/c_{ia} is typically below the threshold of current-driven instability. Thus, we do not expect the currents to be strong enough to trigger IAWs for Maxwellian proton and electron VDFs.

3.3. Analysis of Velocity Distribution Functions

Since the estimated currents alone are not strong enough to excite waves due to drifts between proton and electron Maxwellian distributions, more complex particle distributions are required to generate IAWs. We examine the proton and electron VDFs of two IP shocks, presented in Figure 4. In both cases, the plots are centered on the shock. We show the 1D reduced ion VDF along the radial direction V_R in panels (b, j). For electrons, we show PADs for energies $E > 70$ eV in panels (c, k). We observe a strong asymmetry between electrons parallel and anti-parallel to **B** for the shock in the left panels, likely due to the strahl. For the shock in the right panels, the density of suprathermal electrons upstream of the shock is lower, with only a small dependence on the pitch angle. Panels (d, l) show the electric fields from the TSWF containing IAWs and the maximum amplitudes in the STAT packets containing IAWs. In both events, the waves are predominantly field-aligned, with the largest amplitude waves reaching ~5 mV/m. We observe IAWs clustered at the ramp of both IP shocks, with amplitudes decreasing with increasing distance from the ramp in both directions. In panel (d), the upstream IAW activity is enhanced and is reduced in the downstream region. In panel (l), the upstream IAW activity is significantly lower than downstream.
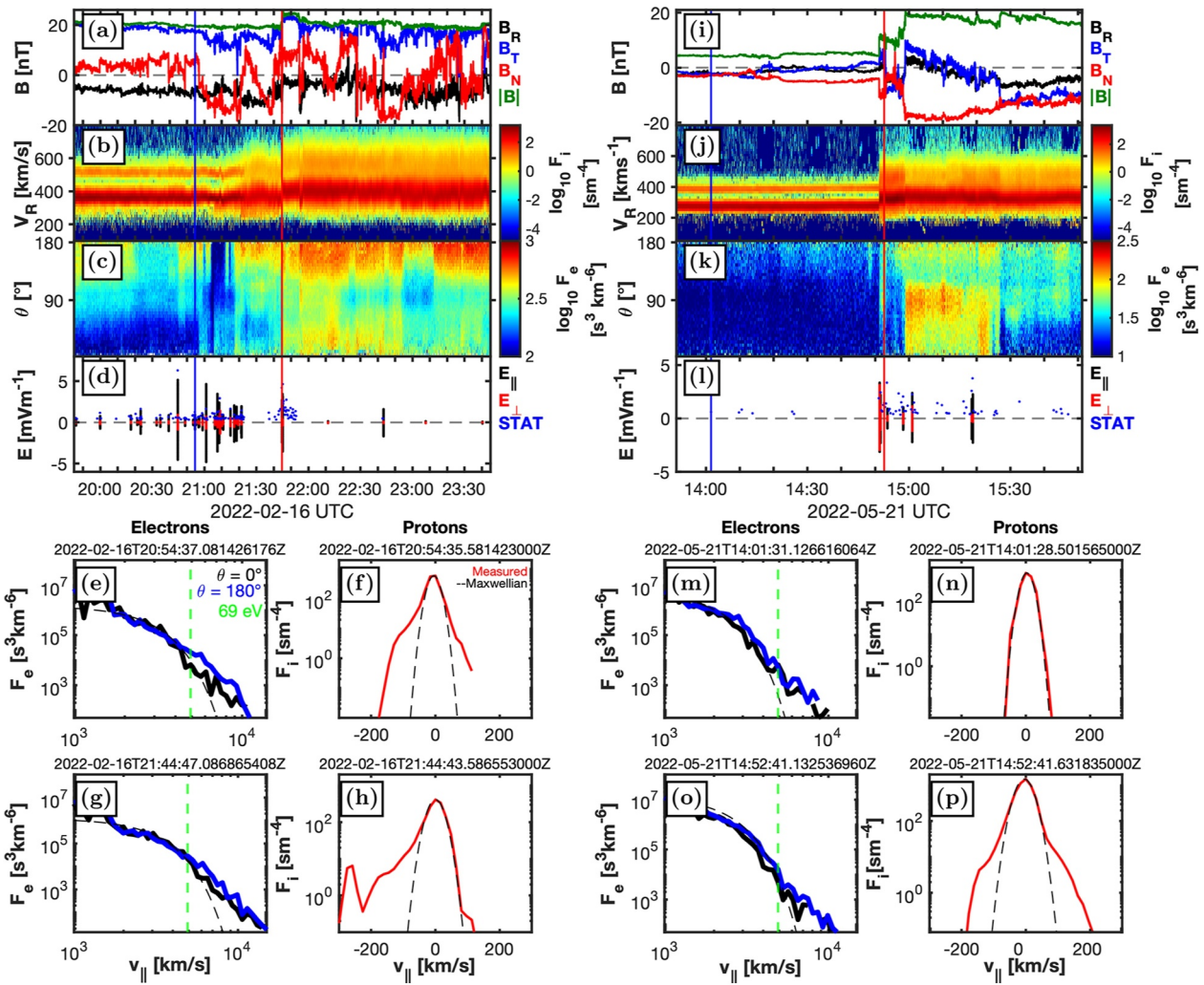
Figure 4. Overview and distribution functions of two different IP shocks. The overview plots are centered on the IP shock. (a, i) Magnetic field RTN components and magnitude. (b, j) Ion velocity distribution function (VDF) along the radial direction. (c, k) Electron pitch angle distribution. (d, l) Electric field snapshots in **B**-field-aligned components and maximum amplitude from STAT packets containing Ion-acoustic waves. (e, m) Electron VDF at $\theta = 0°$ and $\theta = 180°$ at upstream times indicated by the blue vertical lines. Electrons with velocities below the green-dashed line are affected by spacecraft potential effects. (f, n) 1D reduced ion VDF along **B** at upstream times indicated by the blue vertical lines. α-particles have been removed from these distributions. (g, o) Electron VDF at $\theta = 0°$ and $\theta = 180°$ at near-ramp/downstream times indicated by the red vertical lines. (h, p) 1D reduced ion VDF along **B** at near-ramp/downstream times indicated by the red vertical lines. α-particles are not removed from these distributions. Maxwellian distributions are plotted with dashed lines on panels (e–h) and (m–p) for comparison.

Since heat fluxes are generally carried by electrons (Treumann & Baumjohann, 1997), any asymmetry between the electron VDFs at pitch angles $\theta = 0°$ and 180° indicates a heat flux that can potentially trigger IAWs. We analyze the distributions at pitch angles of $\theta = 0°$ and 180° at different times (shown in Figures 4e, 4g, 4m, and 4o). The green-dashed line marks the energy at which the measurements become unreliable due to photoelectron contamination. We focus only on energies above this value, corresponding to the suprathermal electrons.

The largest deviation from a symmetric distribution is in the distribution in Figure 4e, where the average ratio between the anti-parallel and parallel VDFs above 70 eV $\langle v_{-\parallel}/v_{\parallel}\rangle_{>70eV} \sim 4$. We interpret this enhancement in anti-parallel VDF as the strahl population. In addition, we observe high IAW activity in the same region. Closer to the shock (Figure 4g), the asymmetry in the electron distribution is reduced to $\langle v_{-\parallel}/v_{\parallel}\rangle_{>70eV} < 2$, decreasing the electron heat flux. In the case without upstream IAW activity, in Figure 4m, there are no signs of a strahl. From these observations, the presence of upstream IAWs correlates to electron heat fluxes. Whether these heat fluxes are large enough to excite IAW remains to be investigated. In the ramp and downstream regions, there are some IAWs, but no clear strahl (panel o).

We also look for evidence of ion-acoustic instability drivers in the proton distributions. We show the one-dimensional reduced distributions along **B** in Figures 4f, 4h, 4n, and 4p. For the upstream distributions in panels (f, n), we removed the α-particles, as they have well-separated energies from the protons, as seen in panels (b, j). For the distributions closer to the ramp (panels h, p), we could not isolate and remove the α-particles.

The proton distribution in Figure 4f consists of a core population and a shoulder population streaming anti-parallel to **B**. At the same time, many IAWs are observed. The proton distribution in Figure 4n, is approximately Maxwellian along **B**, and no IAWs are observed. Proton beams are known sources of ion-acoustic instabilities (Gary, 1978). However, there are no clear signs of an unstable distribution in Figure 4f, namely a positive slope in the VDF. Since PAS delivers one distribution every 4 s, the minimum between two population peaks is probably not resolved if the distribution fluctuates at shorter time scales.

4. Discussion

From the ion VDF analysis presented above, we see a correlation between upstream IAW activity and two-stream proton distribution. Ion distributions consisting of a proton core and a field-aligned shoulder, like in Figure 4f, are frequently observed in the solar wind, irrespective of the presence of shocks. Moreover, they are often found near high IAW activity regions (Gurnett & Frank, 1978), suggesting that the waves found upstream of the shock in panel (d) correlate with solar wind two-stream protons, rather than the physics of the IP shock. Although the presence of IP shocks is correlated with increased OR, as shown in Figure 2, we conclude that the IP shocks are not responsible for the enhancement in the upstream region. Instead, the solar wind proton and electron VDFs dictate the IAW activity, and the shock has a minor effect on the upstream OR. This explains the poor correlation between shock parameters and upstream OR. Furthermore, the correlation of upstream OR with heliocentric distance can be explained by a general increase of solar wind IAW OR with decreasing distance to the Sun (Píša et al., 2021). The high variability in upstream OR between IP shocks is more likely due to the variable solar wind conditions with two-stream protons and the electron strahl VDFs (Owen et al., 2022; Verscharen et al., 2019).

In the ramp and near-ramp downstream regions, we cannot explain ion-acoustic instability through heat fluxes. Nevertheless, in these regions, we often observe large current density spikes. Although these currents are not large enough to produce the required drifts by themselves, the multi-proton distributions may influence the instability thresholds. For a given temperature ratio of electrons and core protons, the threshold for the ion-acoustic instability associated with a proton beam is increased as the temperature ratio between the beam and the proton core increases (Gary, 1993; Gary & Omidi, 1987). If the shock heats the drifting proton population more than the core, the threshold for ion-acoustic instability will increase. This may explain why the IAW activity is mitigated after the shock ramp in the case of Figures 4a–4h). However, a conclusion cannot be drawn from the available ion distribution measurements in the ramp and downstream regions as the different proton components and α-particles are not well distinguishable.

Additionally, some waves in the downstream region close to the ramp may be IAWs generated at the ramp and convected downstream. This could explain the enhancement of downstream average OR close to the ramp, and is supported by the downstream waves close to the ramp having similar properties to those at the ramp, such as frequency and amplitude (Figures 2b and 2c).

5. Conclusion

We have investigated statistically the occurrence rate of IAWs in the vicinity of 80 IP shocks observed by SolO between 0.3 and 1.1 AU. Our main results are:

- Ion-acoustic waves are a common feature of IP shocks. We observe enhanced IAW activity at the ramp of 84% of the IP shocks. The occurrence rate of IAWs is statistically highest at the shock ramp, where it can reach values almost three orders of magnitude larger than the background solar wind.
- The occurrence rate in the upstream region of IP shocks increases with decreasing distance from the Sun. In this region, the occurrence rate is variable between shocks and can be higher than the background more than 200 min before the shock, however, IP shocks are not the main drivers of IAWs in this region. In the downstream region, the occurrence rate decreases more rapidly and closer to the ramp.
- IAW activity tends to be associated with enhanced currents, although the currents are not strong enough to trigger IAW growth assuming Maxwellian electron and proton distributions. We observe two-streaming

protons and the electron strahl together with IAWs in the upstream region of the analyzed IP shock. These observations suggest a relationship between IAWs and non-Maxwellian proton and electron distributions.

Data Availability Statement

Solar Orbiter is a space mission of international collaboration between ESA and NASA. Solar Orbiter data are available at http://soar.esac.esa.int/soar/. For electric field measurements, we used RPW snapshot data sets (Maksimovic, 2020). For ion and electron data, we use SWA data sets (Owen, 2020). For magnetic field measurements, we used normal mode MAG data sets (Horbury, 2020). The list of IP shocks is available at https://zenodo.org/records/11091062 (Dimmock, 2024).

References

Alterman, B. L., Kasper, J. C., Stevens, M. L., & Koval, A. (2018). A comparison of alpha particle and proton beam differential flows in collisionally young. *Solar Wind*, *864*(2), 112. https://doi.org/10.3847/1538-4357/aad23f

Bale, S. D., Hull, A., Larson, D. E., Lin, R. P., Muschietti, L., Kellogg, P. J., et al. (2002). Electrostatic turbulence and debye-scale structures associated with electron thermalization at collisionless shocks. *The Astrophysical Journal*, *575*(1), L25–L28. https://doi.org/10.1086/342609

Briand, C. (2009). Plasma waves above the ion cyclotron frequency in the solar wind: A review on observations. *Nonlinear Processes in Geophysics*, *16*(2), 319–329. https://doi.org/10.5194/npg-16-319-2009

Christoffersen, G. B., Jensen, V. O., & Michelsen, P. (1974). Investigation of ion acoustic waves in collisionless plasmas. *The Physics of Fluids*, *17*(2), 390–399. https://doi.org/10.1063/1.1694728

Dimmock, A. P. (2024). Solar orbiter IRFU interplanetary shock list [Dataset]. https://doi.org/10.5281/zenodo.11091062

Dimmock, A. P., Gedalin, M., Lalti, A., Trotta, D., Khotyaintsev, Y. V., Graham, D., et al. (2023). Backstreaming ions at a high Mach number interplanetary shock. Solar Orbiter measurements during the nominal mission phase. *Astronomy & Astrophysics*, *679*, A106. https://doi.org/10.1051/0004-6361/202347006

Fitzenreiter, R. J., Ogilvie, K. W., Bale, S. D., & Viñas, A. F. (2003). Modification of the solar wind electron velocity distribution at interplanetary shocks. *Journal of Geophysical Research*, *108*(A12), 1415. https://doi.org/10.1029/2003JA009865

Forslund, D. W. (1970). Instabilities associated with heat conduction in the solar wind and their consequences. *Journal of Geophysical Research*, *75*(1), 17–28. https://doi.org/10.1029/JA075i001p00017

Fried, B. D., & Gould, R. W. (1961). Longitudinal ion oscillations in a hot plasma. *The Physics of Fluids*, *4*(1), 139–147. https://doi.org/10.1063/1.1706174

Gary, S. P. (1978). Ion-acoustic-like instabilities in the solar wind. *Journal of Geophysical Research*, *83*(A6), 2504–2510. https://doi.org/10.1029/JA083iA06p02504

Gary, S. P. (1993). *Theory of space plasma microinstabilities* (1st ed.). Cambridge University Press.

Gary, S. P., & Omidi, N. (1987). The ion-ion acoustic instability. *Journal of Plasma Physics*, *37*(1), 45–61. https://doi.org/10.1017/S0022377800011983

Goldstein, B. E., Neugebauer, M., Zhang, L. D., & Gary, S. P. (2000). Observed constraint on proton-proton relative velocities in the solar wind. *Geophysical Research Letters*, *27*(1), 53–56. https://doi.org/10.1029/1999GL003637

Graham, D. B., Khotyaintsev, Y. V., Vaivads, A., Edberg, N. J. T., Eriksson, A. I., Johansson, E., et al. (2021). Kinetic electrostatic waves and their association with current structures in the solar wind. *Astronomy & Astrophysics*, *656*, A23. https://doi.org/10.1051/0004-6361/202140943

Gurnett, D. A., & Anderson, R. R. (1977). Plasma wave electric fields in the solar wind: Initial results from Helios 1. *Journal of Geophysical Research*, *82*(4), 632–650. https://doi.org/10.1029/JA082i004p00632

Gurnett, D. A., & Bhattacharjee, A. (2017). *Introduction to plasma physics: With space, laboratory and astrophysical applications* (2nd ed.). Cambridge University Press.

Gurnett, D. A., & Frank, L. A. (1978). Ion acoustic waves in the solar wind. *Journal of Geophysical Research*, *83*(A1), 58–74. https://doi.org/10.1029/JA083iA01p00058

Gurnett, D. A., Marsch, E., Pilipp, W., Schwenn, R., & Rosenbauer, H. (1979). Ion acoustic waves and related plasma observations in the solar wind. *Journal of Geophysical Research*, *84*(A5), 2029–2038. https://doi.org/10.1029/ja084ia05p02029

Hess, R. A., MacDowall, R. J., Goldstein, B., Neugebauer, M., & Forsyth, R. J. (1998). Ion acoustic-like waves observed by Ulysses near interplanetary shock waves in the three-dimensional heliosphere. *Journal of Geophysical Research*, *103*(A4), 6531–6541. https://doi.org/10.1029/97ja03395

Horbury, T. S. (2020). MAG, Solar Orbiter magnetometer, level 2 (L2) MAG normal mode magnetic field in RTN coordinates (L2-mag-rtn-normal) [Dataset]. *European Space Agency*. https://doi.org/10.5270/esa-ux7y320

Horbury, T. S., O'Brien, H., Blazquez, I. C., Bendyk, M., Brown, P., Hudson, R., et al. (2020). The solar orbiter magnetometer. *Astronomy & Astrophysics*, *642*, A9. https://doi.org/10.1051/0004-6361/201937257

Khotyaintsev, Y. V., Graham, D. B., Vaivads, A., Steinvall, K., Edberg, N. J. T., Eriksson, A. I., et al. (2021). Density fluctuations associated with turbulence and waves. *Astronomy & Astrophysics*, *656*, A19. https://doi.org/10.1051/0004-6361/202140936

Kilpua, E. K., Lumme, E., Andreeova, K., Isavnin, A., & Koskinen, H. E. (2015). Properties and drivers of fast interplanetary shocks near the orbit of the earth (1995–2013). *Journal of Geophysical Research: Space Physics*, *120*(6), 4112–4125. https://doi.org/10.1002/2015JA021138

Kurth, W., Craven, J., Frank, L., & Gurnett, D. (1979). Intense electrostatic waves near the upper hybrid resonance frequency. *Journal of Geophysical Research*, *84*(A8), 4145–4164. https://doi.org/10.1029/JA084iA08p04145

Lalti, A., Khotyaintsev, Y. V., & Graham, D. B. (2023). Short-wavelength electrostatic wave measurement using mms spacecraft. *Journal of Geophysical Research: Space Physics*, *128*(4). https://doi.org/10.1029/2022JA031150

Lotekar, A. B., Vasko, I. Y., Phan, T., Bale, S. D., Bowen, T. A., Halekas, J., et al. (2022). Kinetic-scale current sheets in near-sun solar wind: Properties, scale-dependent features and reconnection onset. *The Astrophysical Journal*, *929*(1), 58. https://doi.org/10.3847/1538-4357/ac5bd9

Maksimovic, M. (2020). RPW, Radio and Plasma Waves instrument, level 2 (L2) TDS electric field triggered snapshot waveforms (rpw-tds-surv-tswf-e) and STAT statistical product of electric field continuous snapshots rpw-tds-surv-stat [Dataset]. *European Space Agency*. https://doi.org/10.57780/esa-3xcjd4w

Maksimovic, M., Bale, S. D., Chust, T., Khotyaintsev, Y., Krasnoselskikh, V., Kretzschmar, M., et al. (2020). The solar orbiter radio and plasma waves (RPW) instrument. *Astronomy & Astrophysics*, *642*, A12. https://doi.org/10.1051/0004-6361/201936214

Müller, D., Cyr, O. C. S., Zouganelis, I., Gilbert, H. R., Marsden, R., Nieves-Chinchilla, T., et al. (2020). The solar orbiter mission. *Astronomy & Astrophysics*, *642*, A1. https://doi.org/10.1051/0004-6361/202038467

Newbury, J. A., Russell, C. T., Phillips, J. L., & Gary, S. P. (1998). Electron temperature in the ambient solar wind: Typical properties and a lower bound at 1 au. *Journal of Geophysical Research*, *103*(A5), 9553–9566. https://doi.org/10.1029/98ja00067

Owen, C. J. (2020). The Solar Orbiter Solar Wind Analyser (SWA) suite, level 2 (L2) PAS velocity distribution functions (swa-pas-vdf), PAS ground calculated moments (swa-pas-grnd-mom) and EAS single strahl electron distribution data product (eas[1/2]-ss-psd) [Dataset]. *European Space Agency*. https://doi.org/10.5270/esa-ahypgn6

Owen, C. J., Abraham, J. B., Nicolaou, G., Verscharen, D., Louarn, P., & Horbury, T. S. (2022). Solar orbiter SWA observations of electron Strahl properties inside 1 AU. *Universe*, *8*(10), 509. https://doi.org/10.3390/universe8100509

Owen, C. J., Bruno, R., Livi, S., Louarn, P., Janabi, K. A., Allegrini, F., et al. (2020). The solar orbiter solar wind analyser (swa) suite. *Astronomy & Astrophysics*, *642*, A16. https://doi.org/10.1051/0004-6361/201937259

Píša, D., Souček, J., Santolík, O., Hanzelka, M., Nicolaou, G., Maksimovic, M., et al. (2021). First-year ion-acoustic wave observations in the solar wind by the RPW/TDS instrument onboard solar orbiter. *Astronomy & Astrophysics*, *656*, A14. https://doi.org/10.1051/0004-6361/202140928

Soucek, J., Píša, D., Kolmasova, I., Uhlir, L., Lan, R., Santolík, O., et al. (2021). Solar orbiter radio and plasma waves - Time domain sampler: In-flight performance and first results. *Astronomy and Astrophysics*, *656*, A26. https://doi.org/10.1051/0004-6361/202140948

Treumann, R. A., & Baumjohann, W. (1997). *Advanced space plasma physics* (1st ed.). Imperial College Press.

Vasko, I. Y., Alimov, K., Phan, T., Bale, S. D., Mozer, F. S., & Artemyev, A. V. (2022). Kinetic-scale current sheets in the solar wind at 1 au: Scale-dependent properties and critical current density. *The Astrophysical Journal Letters*, *926*(2), L19. https://doi.org/10.3847/2041-8213/ac4fc4

Verscharen, D., Klein, K. G., & Maruca, B. A. (2019). The multi-scale nature of the solar wind. *Living Reviews in Solar Physics*, *16*(1), 5. https://doi.org/10.1007/s41116-019-0021-0

Wilson, L. B., Cattell, C., Kellogg, P. J., Goetz, K., Kersten, K., Hanson, L., et al. (2007). Waves in interplanetary shocks: A wind/waves study. *Physical Review Letters*, *99*(4), 041101. https://doi.org/10.1103/PhysRevLett.99.041101